IOP Conference Series: Materials
Science and Engineering

Failure Prediction in Fiber Metal Laminates for Next Generation Aero Materials

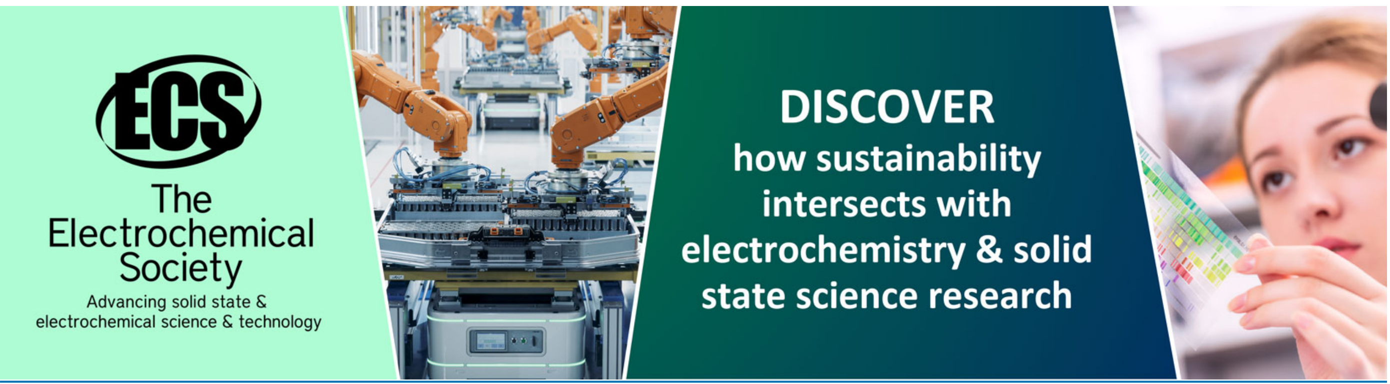

Failure Prediction in Fiber Metal Laminates for Next Generation Aero Materials

H Jeevan Rao[1], Perumalla Janaki Ramulu[2], M Vishnu Vardhan[3], CH Chandramouli[3]

[1]Department of Aerospace Engineering,Vardhaman College of Engineering, Shamshabad, 501218, India

[2]School of Mechancial, Chemical and Materials Engineering. Adama Science and Technology University, Adama, Ethiopia, P.Box:1888

[3] Department of Mechanical engineering, Vardhaman College of Engineering, Shamshabad, 501218, India

Email: perumalla.janaki@astu.edu.et

Abstract. In aerospace industry, there is huge demand for low density and low cost materials with better mechanical properties. In this view, there are many researchers developed new materials interms of composites. Similar manner, the present paper also aimed to produce a new approach for cost effective materials of 3D weaved glass fiber metal laminates (FML) with different compositions using a numerical study. A method for the simulation of progressive delamination based on de-cohesion elements has been presented. De-cohesion elements are placed between layers of solid elements that open and shear in response to the loading situation. The onset of damage and the growth of delamination are simulated without previous knowledge about the location, the size, or the direction of propagation of the de-laminations. A softening law for mixed-mode delamination that can be applied to any interaction criterion is also proposed. The constitutive equation proposed uses a single variable, the maximum relative displacement, to track the damage at the interface under general loading conditions. The material properties required to define the element constitutive equation are the inter-laminar fracture toughness's, the penalty stiffness, and the strengths.

Keywords: Fiber metal laminates (FML); Epoxy resin, Metal matrix; Aluminum and Glass fiber

1. Introduction

For the past few decades, the application of fibrous composite materials in engineering applications has become increasingly popular, especially in the aeronautical and space sector. Their plethora of uses in both military and civil aircraft also extends to applications that are more exotic. Their growing utilities have arisen from a drive within the aerospace industry to produce light weight aircraft, as the cost of fuel increases and environmental awareness becomes an important consideration. Composites are preferred over the conventional materials, such as steel and aluminum, because of their strength/stiffness versus weight ratio and the ability to shape and tailor structures to produce more aerodynamically efficient structural configurations. However, reducing the weight and maintaining the structural integrity, affordability and durability continues to be a major issue in aircraft design. The manufacturing process, assembly process and performance of composites are well connected. However, metallic materials and their derivatives continue to have a fundamental role in applications where composites have yet to be exploited. This led to the development of a hybrid system partly made of fibrous composites, known as fiber metal laminates (FMLs). FMLs consist of alternating

layers of thin metallic sheets and fiber-reinforced plastics. Composite materials have been subject of permanent interest of various specialists during the last decades. Firstly, military applications in the aircraft industry triggered off the commercial use of composites after the Second World War. The innovations in the composite area have allowed significant weight reduction in structural design. Composites offer many advantages when compared to metallic alloys, especially where high strength and stiffness to weigh ratio is concerned. Additionally, they provide excellent fatigue properties and corrosion resistance in applications [1]. With all these advantages, composite structures have gained widespread use in the aerospace industry during the last decades [2–6].
The mechanical behavior of composite bolted joints has been extensively studied in the past by means of experimental, analytical and numerical approaches [7-11], mainly focusing on the determination of the load capability, the load and stress distributions and failure criteria of single- and multi-row bolted joints under the influence of varying laminate configurations and joint geometries. One of the most effective ways to improve the load capacity of composite bolted joints entails the local reinforcement of the composite laminate with high-strength metal layers [12-16], thus clearly improving its bearing and shear capabilities. The special feature of this reinforcement technique consists of only embedding the metal layers into the bolted joining area locally, which is accomplished either byply-addition (metallic layers are inserted between the composite plies) or ply-substitution techniques (composite plies are replaced by metallic layers). Hence, the total load capability of this reinforcement approach depends not only directly on the load capability of the bolted joint, but also on the strength of the transition zone between the pure fiber composite material and the hybridized laminate region multiple layers of thin aluminum alloy sheets [17-20]. From the all the studies, it was understood that the essentiality of the new composites for structural applications is must. The present study aimed the new generation fiber metal laminates numerical simulation for aerospace industry.

2. Methodology

2.1 Code Development

Considering the dynamic nature of reiterations involved in the present paper, it has been decided to use Salome and Code Aster available as open source code in CAE Linux. As both were written in Fortran and python they provide end users with flexibility to define the boundaries in much detail.
As first step of modeling, the SI unit system was followed for local and global systems. Geometrical configuration and boundary values were mentioned in the Table 1 and 2. Figure 1 shows the composite layer with mentioned geometrical and boundaries indicated in the Table 1 and 2.

Table 1 Boundaries for layer

Property	Value
Space dimension	3
Number of domains	6
Number of boundaries	29
Number of edges	46
Number of vertices	24

Table 2 Geometrical details of layer

Name	Value
Width	cl
Depth	wb/2
Height	Hb
Layer 1	hb/2

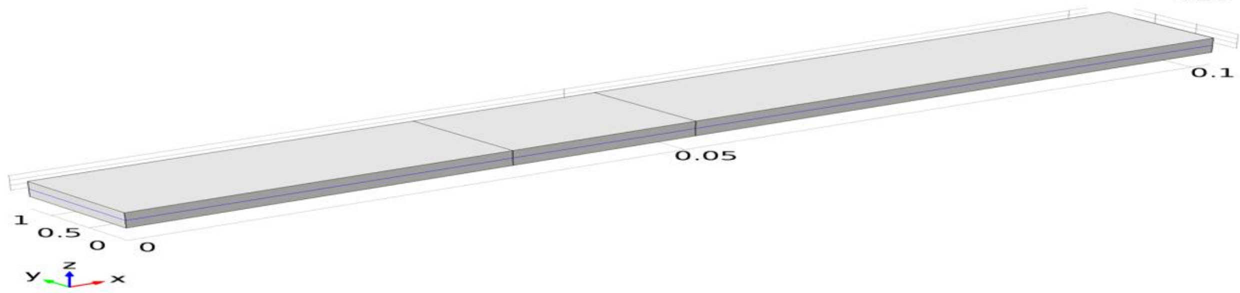

Figure 1. Composite layer 1

Table 3 Composite layers details used for coding

Name	Expression	Value	Description
lb	102[mm]	0.10200 m	Length
wb	25.4[mm]	0.025400 m	Width
hb	2×1.56[mm]	0.0031200 m	Thickness
cl	34.1[mm]	0.034100 m	Initial crack length
Kp	1e6[N/mm^3]	1.0000E15 N/m³	Penalty Stiffness
N_strength	80[MPa]	8.0000E7 Pa	Normal Tensile Strength
S_strength	100[MPa]	1.0000E8 Pa	Shear Strength
u_I_0	N_strength/Kp	8.0000E-8 m	Mode I failure initiation displacement
u_II_0	S_strength/Kp	1.0000E-7 m	Model II failure initiation displacement
GIc	0.969[kJ/m^2]	969.00 J/m²	Mode I critical energy release
GIIc	1.719[kJ/m^2]	1719.0 J/m²	Mode II critical energy release
u_I_f	2×GIc/N_strength	2.4225E-5 m	Mode I ultimate displacement
u_II_f	2×GIIc/S_strength	3.4380E-5 m	Mode II ultimate displacement
eta	2.284	2.2840	Exponent of Benzeggagh and Kenane (B-K) criterion
disp	0	0.0000	Displacement parameter
mm	0.5	0.50000	Mode mixity ratio
ll	lb/2× (0.5×sqrt(3× (1 - mm)/mm) + 1)/(3 - 0.5×sqrt(3× (1 - mm)/mm))	0.044596 m	Lever length
lr	8× ((6mm + sqrt(3mm(1 mm)))/(3 + 9×mm + 8×sqrt(3mm(1 - mm))))	2.1436	Load ratio middle/cracked edge

Table 4 Cohesive Zone Definition

Name	Expression	Description
u_I	-solid.uspring3_tel1	Normal relative displacement
u_II	sqrt(solid.uspring1_tel1^2 + solid.uspring2_tel1^2)	Total tangential relative displacement
u_m	sqrt(u_II^2 + u_I^2)	Mixed mode relative displacement
u_max	max(u_max_old, u_m)	Maximum mixed mode relative displacement
beta	if(u_I>0, u_II/u_I, 0)	Mode mixity
u_m_0	if(u_I>0, u_I_0×u_II_0×sqrt((1 + beta^2)/(u_II_0^2 + (beta×u_I_0)^2)), u_II_0)	Mixed mode damage initiation
u_m_f	if(u_I>0,2/Kp/u_m_0×(GIc+(GIIc-GIc)× ((beta^2/(1 + beta^2))^eta)), sqrt(2) ×u_II_f)	Mixed mode total de-cohesion displacement
damage	u_m_f×(nojac(u_max)-u_m_0)/(nojac(u_max)× (u_m_f - u_m_0))	Damage evolution function

stiffness	if(u_max<u_m_0,Kp,if(u_max>u_m_f,0,(1-damage)×Kp))	Thin elastic layer stiffness

Table 5 Load Definition

Name	Expression	Description
u_lp	(3×ll-lb/2)/4/(lb/2)×intop1(u_I)+((ll+ lb/2)/(lb/2))×(intop2(-w) + intop1(u_I)/4)	Load point displacement
F_lp	force×lb/2/ll	Load point force

Table 6 Mechanical Properties used for whole composite

Name	Value	Unit
Density	1570	kg/m^3
Young's modulus	{122.7e9, 10.1e9, 10.1e9}	Pa
Poisson's ratio	{0.25, 0.45, 0.25}	1
Shear modulus	{5.5e9, 3.7e9, 5.5e9}	N/m^2

Table 3 data indicates the complete data that used for the coding. It showed the entire the geometrical and boundary conditions of the composite layer. Similarly, cohesive zone details were showed in the Table 4. Table 5 and 6 load details and mechanical properties of composite layers and cohesive zone. Loss factor for both young modulus and shear modulus was considered as zero for both composite layers and cohesive zones.

Equation 1 was a characteristic equation used for the simulation

$$-\nabla.\sigma = F_v \text{ ------- [1]}$$

The simulation settings were indicated in the Table 7. A quadratic displacement field was used by keeping boundary fluxes off during simulation. Table 8 indicated the variables used in coding.

Table 7. Simulation settings

Description	Value
Displacement field	Quadratic
Compute boundary fluxes	Off
Value type when using splitting of complex variables	Complex
Structural transient behavior	Include inertial terms
Reference point for moment computation, x component	0
Reference point for moment computation, y component	0
Reference point for moment computation, z component	0
Typical wave speed for perfectly matched layers	solid.cp

Table 8. Variables details in the coding

Name	Expression	Unit	Description	Selection
solid.nX	nX	1	Normal vector, X component	Boundaries 6, 10, 13, 15, 19, 22, 24
solid.nY	nY	1	Normal vector, Y component	Boundaries 6, 10, 13, 15, 19, 22, 24
solid.nZ	nZ	1	Normal vector, Z component	Boundaries 6, 10, 13, 15, 19, 22, 24
solid.nX	dnX	1	Normal vector, X component	Boundaries 1–5, 7–9, 11–12, 14, 16–18, 20–21, 23, 25–29
solid.nY	dnY	1	Normal vector, Y component	Boundaries 1–5, 7–9,

IOP Conf. Series: Materials Science and Engineering **149** (2016) 012102 doi:10.1088/1757-899X/149/1/012102

				11–12, 14, 16–18, 20–21, 23, 25–29
solid.nZ	dnZ	1	Normal vector, Z component	Boundaries 1–5, 7–9, 11–12, 14, 16–18, 20–21, 23, 25–29
solid.nx	nx	1	Normal vector, x component	Boundaries 6, 10, 13, 15, 19, 22, 24
solid.ny	ny	1	Normal vector, y component	Boundaries 6, 10, 13, 15, 19, 22, 24
solid.nz	nz	1	Normal vector, z component	Boundaries 6, 10, 13, 15, 19, 22, 24
solid.nx	dnx	1	Normal vector, x component	Boundaries 1–5, 7–9, 11–12, 14, 16–18, 20–21, 23, 25–29
solid.ny	dny	1	Normal vector, y component	Boundaries 1–5, 7–9, 11–12, 14, 16–18, 20–21, 23, 25–29
solid.nz	dnz	1	Normal vector, z component	Boundaries 1–5, 7–9, 11–12, 14, 16–18, 20–21, 23, 25–29
solid.nXmesh	root.nXmesh	1	Normal vector (mesh), X component	Boundaries 6, 10, 13, 15, 19, 22, 24
solid.nYmesh	root.nYmesh	1	Normal vector (mesh), Y component	Boundaries 6, 10, 13, 15, 19, 22, 24
solid.nZmesh	root.nZmesh	1	Normal vector (mesh), Z component	Boundaries 6, 10, 13, 15, 19, 22, 24
solid.nXmesh	root.dnXmesh	1	Normal vector (mesh), X component	Boundaries 1–5, 7–9, 11–12, 14, 16–18, 20–21, 23, 25–29
solid.nYmesh	root.dnYmesh	1	Normal vector (mesh), Y component	Boundaries 1–5, 7–9, 11–12, 14, 16–18, 20–21, 23, 25–29
solid.nZmesh	root.dnZmesh	1	Normal vector (mesh), Z component	Boundaries 1–5, 7–9, 11–12, 14, 16–18, 20–21, 23, 25–29
solid.nxmesh	root.nxmesh	1	Normal vector (mesh), x component	Boundaries 6, 10, 13, 15, 19, 22, 24
solid.nymesh	root.nymesh	1	Normal vector (mesh), y component	Boundaries 6, 10, 13, 15, 19, 22, 24
solid.nzmesh	root.nzmesh	1	Normal vector (mesh), z component	Boundaries 6, 10, 13, 15, 19, 22, 24
solid.nxmesh	root.dnxmesh	1	Normal vector (mesh), x component	Boundaries 1–5, 7–9, 11–12, 14, 16–18, 20–21, 23, 25–29
solid.nymesh	root.dnymesh	1	Normal vector (mesh), y component	Boundaries 1–5, 7–9, 11–12, 14, 16–18, 20–21, 23, 25–29
solid.nzmesh	root.dnzmesh	1	Normal vector (mesh), z component	Boundaries 1–5, 7–9, 11–12, 14, 16–18, 20–21, 23, 25–29
solid.refpntx	0	m	Reference point for moment computation, x component	Global

solid.refpnty	0	m	Reference point for moment computation, y component	Global
solid.refpntz	0	m	Reference point for moment computation, z component	Global
solid.cref	solid.cp	m/s	Typical wave speed for perfectly matched layers	Domains 1–6
xt	d(x,TIME)	m/s	Mesh velocity, x component	Global
yt	d(y,TIME)	m/s	Mesh velocity, y component	Global
zt	d(z,TIME)	m/s	Mesh velocity, z component	Global

Similarly for second layer also defined for data evaluation as shown in the Figure 2. Equations 2 to 5 were used for the simulation. Figure 3 shows the meshed geometry of the composite layers and the mesh details were indicated in table 9 including the boundary conditions.

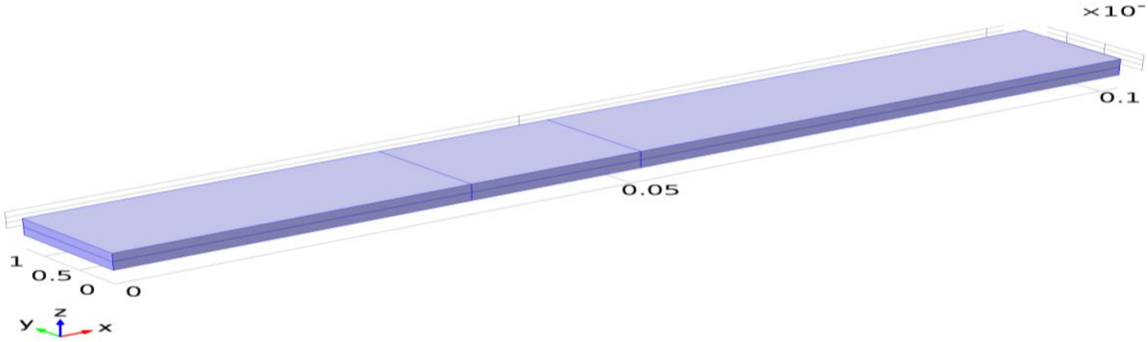

Figure 2. Composite layer 2

$$0 = \nabla.(\mathrm{FS}) + \mathrm{F}_v \qquad [2]$$

$$\mathrm{F}=\mathrm{I}+\nabla u \qquad [3]$$

$$s = s_0 + C:(\varepsilon - \varepsilon_0 - \varepsilon_{inel}) \qquad [4]$$

$$\varepsilon = \frac{1}{2}(\nabla u + (\nabla u)^T + (\nabla u)^T \nabla u) \qquad [5]$$

Then we defined the load as shown in the Equations 6 and 7

$$F = F_L \qquad [6]$$

$$F_L = \frac{F_{tot}}{L} \qquad [7]$$

Using symmetry we define prescribed displacement as

$$w = u_{0Z} \qquad [8]$$

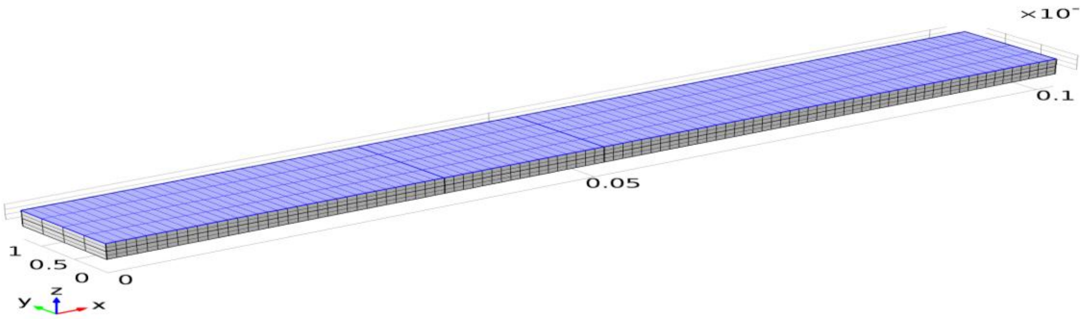

Figure 3. Meshed composite layers along with boundary conditions

Table 9 Details of the mesh and boundary conditions

Name	Value
Maximum element size	0.00204/2
Minimum element size	2.04E-5
Minimum element size	Off
Curvature factor	0.2
Curvature factor	Off
Resolution of narrow regions	Off
Maximum element growth rate	1.3
Maximum element growth rate	Off
Predefined size	Extremely fine
Custom element size	Custom

The program was then prepped for computation by fixing the details shoed in the Table 10.

Table 10 Simulation conditions

Property	Value
Include geometric nonlinearity	On
Physics interface	Discretization
Solid Mechanics (solid)	physics
Boundary ODEs and DAEs (bode)	physics
Geometry	Mesh
Geometry 1 (geom1)	mesh1
Name	Value
Use study	Study 1
Use study step	Stationary
Defined by study step	Stationary
Solution	Zero
Field components	comp1.u_max_old
Field components	{comp1.u, comp1.v, comp1.w}
State components	comp1.force

3. Results and Discussion

An extensive literature review has pointed out the existing approaches and methodologies used to evaluate Advanced Aero material numerically. In current approach, the authors applied the cohesive bond theory to evaluate the bond energy and stresses in the fatigued area to understand the de-lamination dynamics.

The model is computed for a mode ratio of 50%. The von Mises stress distributions are computed using parametric step method. The resultant crack initiated at this stage is represented in using red for de-bonded zone and green for healthy zone. Because of the nonlinearity and history dependence of the CZM, it is necessary to solve the model parametrically. The desired load is applied on the top edges of the beam. The force-displacement curve reveals that the applied forces are not monotonically increasing functions this can be used for the parametric solver.

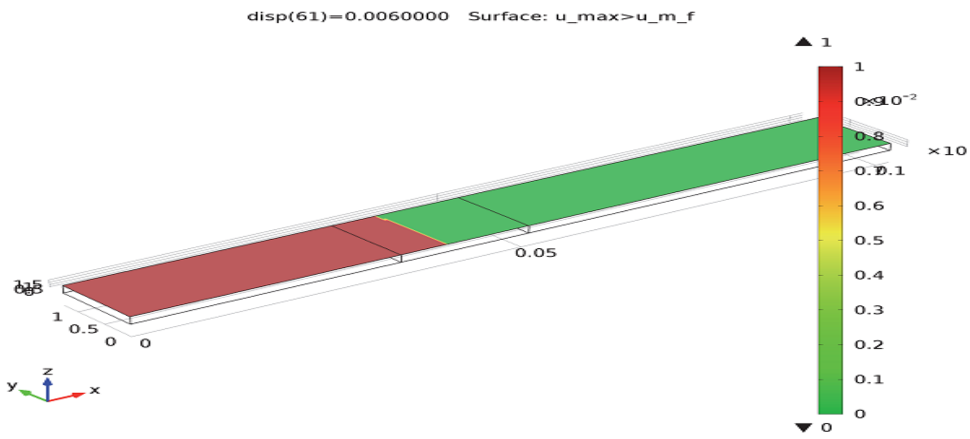

Figure 4. Displacement filed after simulation

To overcome the non- monotonicity in the interface of the joints, we define them using a simple code for the parameters which enable the Python binaries to focus the mesh deformation at the point of study using the formation functions.

One of the outputs of the mixed mode bending test is a load-displacement curve. Both load and displacement are measured at the end point of the lever that is used to apply the load to the test specimen. Since the layer is not explicitly modeled, the load-displacement data has to be deduced from the simulation results. Figure 5 shows the load vs displacement behavior of whole composite bar obtained from the simulation results. It shows, the maximum load is obtained as 255N corresponding 5.44 mm displacement. Finally using the above date, the resultant von Misses Stresses are shown in the Figure 6.

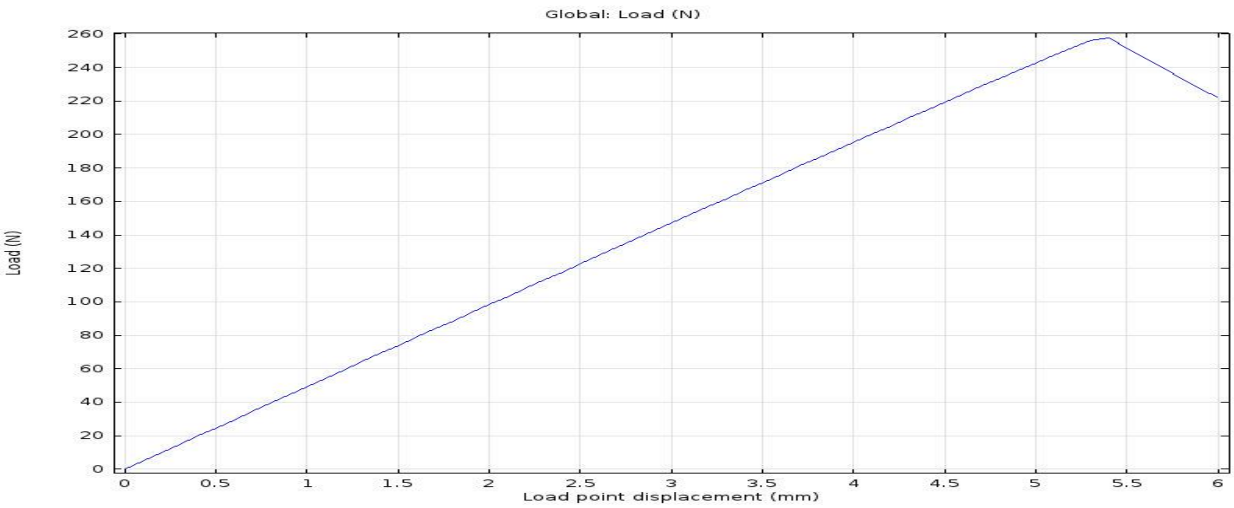

Figure 5. Load vs Displacement behavior of composite bar

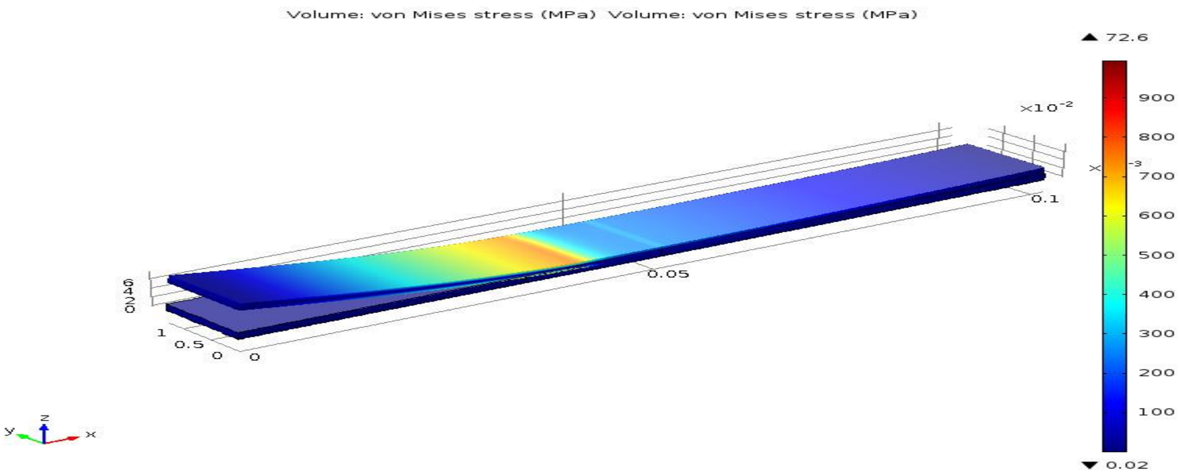

Figure 6. Von-Mises stress indication in the FML

A method for the simulation of progressive de-lamination based on de-cohesion elements is presented in this work. De-cohesion elements are placed between layers of solid elements that open and shear in response to the loading situation. The onset of damage and the growth of de-lamination are simulated without previous knowledge about the location, the size, or the direction of propagation of the de-laminations. A softening law for mixed-mode de-lamination that is applied to any interaction criterion is proposed. The constitutive equation proposed uses a single variable, the maximum relative displacement, to track the damage at the interface under general loading conditions. The material properties required to define the element constitutive equation are the inter-laminar fracture toughness's, the penalty stiffness, and the strengths.

4. Conclusions

FMLs consist of metallic alloy and fibre reinforced prepreg. Mostly available GLARE, ARALL and CARALL consists various aluminium alloys. Many researchers have been trying to use possible metallic alloys such as magnesium, titanium, etc., instead of aluminium alloys. It is expected that this diversity lead optimum mechanical properties.

Same efforts have examined for engineering polymeric materials to replace fibre-reinforced prepreg. New processing methods suggested for improving the productivity of curing process and decreasing the labor costs of FMLs. These improvements will show FMLs very attractive to various industrial applications such as military, automotive and aircraft. By using thermoplastic matrix, FMLs will find new application areas. However, low compatibility of thermoplastic matrix with metal surfaces needs improved by surface modification methods. This study is a simple hypothetical phenomenon to understand the FMLs behavior under different conditions.

References

[1]. Sinmazçelik T, Avcu E, Bora M Ö, Çoban O, 2011 *A review: Fibre metal laminates, background, bonding types and applied test methods*, Materials & Design, *32*(7), pp. 3671-3685.

[2]. Wu G, Yang J M, Hahn H T, 2007, *The impact properties and damage tolerance and of bi-directionally reinforced fiber metal laminates*, Journal of materials science, *42*(3), pp.948-957.

[3]. Mathivanan N R, Jerald J, 2010, *Experimental investigation of low-velocity impact characteristics of woven glass fiber epoxy matrix composite laminates of EP3 grade*, Materials & Design, 31(9), pp. 4553-4560.

.

[4]. Morinière F, Alderliesten R, Tooski M, Benedictus R, 2012, *Damage evolution in GLARE fibre-metal laminate under repeated low-velocity impact tests*, Open Engineering, *2*(4), pp. 603-611.
[5]. Seo H, Hundley J, Hahn H T, Yang J M, 2010, *Numerical simulation of glass-fiber-reinforced aluminum laminates with diverse impact damage*, AIAA journal, 48(3), 676-687.
[6]. Alderliesten R, Benedictus R, 2008, *Fiber/metal composite technology for future primary aircraft structures*, Journal of Aircraft, *45*(4), pp. 1182-1189.
[7]. Seo H, Hundley J, Hahn H T, Yang J M,(2010, *Numerical simulation of glass-fiber-reinforced aluminum laminates with diverse impact damage*, *AIAA journal*, *48*(3), pp. 676-687.
[8]. Botelho E C, Silva R A, Pardini L C, Rezende M C, 2006, *A review on the development and properties of continuous fiber/epoxy/aluminum hybrid composites for aircraft structures*, Materials Research, 9(3), pp. 247-256.
[9]. Bernhardt S, Ramulu M, Kobayashi AS, 2007, *Low-velocity impact response characterization of a hybrid titanium composite laminate*, Journal of Engineering Materials Technology, 129, pp. 220–226.
[10]. Villanueva GR, Cantwell WJ, 2004, *The high velocity impact response of composite and FML-reinforced sandwich structures*, Composites Science and Technology, 64, pp.35–54.
[11]. Beumler T, Pellenkoft F, Tillich A, Wohlers W, Smart C, 2006, *Airbus costumer benefit from fiber metal laminates*, Airbus Deutschland GmbH, Ref. no: L53pr0605135-Issue 1, pp. 1–18.
[12]. Alderliesten R C, Benedictus R, 2007, *Fiber/metal composite technology for future primary aircraft structures*, In: 48th Aiaa/Asme/Asce/Ahs/Asc structures, structural dynamics, and materials conference 15th; April 23–26, Honolulu, Hawaii; 2007. p. 1–12.
[13]. Cortes P, Cantwell W J, 2006, *The prediction of tensile failure in titanium-based thermoplastic fiber–metal laminates,* Composites Science and Technology, 66, pp. 2306–16.
[14]. Asundi A, Choi Alta YN, 1997, *Fiber metal laminates: an advanced material for future aircraft*, Journal of Material Processes and Technology, 63, pp. 384–94.
[15]. Vogelesang LB, Vlot A, 2000, *Development of fiber metal laminates for advanced*, Journal of Material Processes and Technology, 103, pp. 1–5.
[16]. Chang PY, Yeh PC, Yang JM, 2008, *Fatigue crack initiation in hybrid boron/glass/ aluminum fiber metal laminates*, Material Science and Engineering A, 496, pp. 273–80.
[17]. Alderliesten R, 2009, *On the development of hybrid material concepts for aircraft structures*, Recent Patents Engineering, 3, pp. 25–38.
[18]. Remmers J J C, Borst R D, 2001, Delamination buckling of fiber–metal laminates, Composites Science and Technology, 61, pp. 2207–13.
[19]. Schut J, Alderliesten RC, 2006, *De-lamination growth rate at low and elevated temperatures in glare*, In: 25th International congress of the aeronautical sciences, September 3–8; Hamburg, Germany, pp. 1–7.
[20]. Vlot A, 1996, Impact loading on fiber metal laminates, International Journal of Impact Engineering, 18(3), pp. 291–307.